Research on Engineering Structures & Materials
www.jresm.org
MIM Research Group

Research Article

The mechanical behavior of concrete reinforced by non-metallic materials and treated with sawdust ash

Humam Raad Raheem Alazzawi [*,a], K. Rambabu [b]

Dept. of Civil Engineering, Andhra University, College of Engineering, Visakhapatnam-530003, India

Article Info

Article History:

Received 30 Nov 2025

Accepted 20 May 2026

Keywords:

Sawdust ash;
Date palm fiber;
Alkali treatment;
Sustainable concrete;
Mechanical properties;
Regression modelling

Abstract

The concrete industry generates approximately 5-10% of global anthropogenic CO_2 emissions from the production of ordinary Portland cement (OPC), and waste such as wood and date palm agro-residues are largely underutilized. This study fills an existing gap in research by examining the mechanical performance of OPC-based concrete with partial replacement of OPC by sawdust ash (SDA), the resulting concrete reinforced with alkali-treated date palm fiber (DPF), and presents age-specific predictive regression models useful for design. The four levels of SDA use (5%, 10%, 20%, and 30% by mass of cement) and two dosage rates of DPF (0.5% and 1% by mass of binder at the optimum SDA rate) were evaluated. To enhance the fiber–matrix bond, DPF was treated with 3% NaOH for 3 hours and then rinsed to neutral pH. Concrete was proportioned per IS 10262 / IS 8112-1989 with a w/c of 0.45 and cured at 23 ± 2 °C and ≥ 95% relative humidity. The cube strength was determined by three replicate specimens for each mix at 28, 56, and 90 days of testing, as per IS 516. Also, the split tensile strength was determined from three replicates of the mix at each point, and the flexural strength was tested simultaneously using three prism replicates. The data are presented as the mean value with SD. At 90 days, it was found that 5% SDA showed compressive strength (45.43 MPa), tensile strength (5.84 MPa), and flexural strength (5.65 MPa), which was comparable with control (43.67 MPa, 5.43 MPa, and 5.17 MPa), while 30% SDA showed a compressive strength reduction of approximately 43%. The optimum mix (5% SDA + 1% DPF) showed increased CS (3.22%), STS (45.86%), and FS (111%) after 90 days when compared with the reference (5% SDA). The models (R^2 = 0.85-0.96 (linear (SDA)) and R^2 = 0.99-1.00 (exponential (DPF))) were linear and exponential, with high coefficients of determination, and thus could be used to make predictions within the range studied. The added value is the development of a combined SDA–DPF formulation, along with age-resolved statistical characterization and predictive equations, providing an engineer with a realistic foundation for sustainable structures based on the use of locally available agro-industrial wastes.

1. Introduction

The Concrete is the world's most common construction material and is made of cement, fine and coarse aggregates, and water. It involves energy-and carbon-intensive production, and accounts for approximately 5-10% of global anthropogenic CO_2, most of which is emitted from the calcination of limestone and combustion of fuel in the ordinary Portland Cement (OPC) production process [1].

Research to reduce this environmental impact has now been focused on two complementary directions: (i) replacing part of the OPC with pozzolanic by-products that are the by-products of agricultural or industrial activity and (ii) using natural fibers as reinforcement to increase ductility and reduce the brittleness found in low cement concrete.

*Corresponding author: humamr6@gmail.com
[a]orcid.org/0009-0000-8319-4901; [b]orcid.org/0009-0000-2406-8622
DOI: http://dx.doi.org/10.17515/resm2026-1384me1130rs

Sawdust ash (SDA) is one such by-product, which is produced in large volumes by the timber and furniture industry [2]. It contains amorphous silica, alumina, and iron oxide, which satisfy the ASTM C618/IS 3812 pozzolanic requirement if the content of Combined (SiO_2+Al_2O_3+Fe_2O_3) is more than 70% of the mass of the material [3]. Date palm fiber (DPF) is a lignocellulosic waste produced from pruning date palm trees, and there is a huge availability in the arid regions, which is typically disposed of by uncontrolled burning [4]. It has key advantages of biodegradability, being environmentally friendly, easy-to-generate, low-density, and high tensile strength, making it a promising natural reinforcement.

There are several published studies that have studied each of these technologies separately. Increasing replacement of OPC up to 15–20% showed either no decrease or a slight decrease in the compressive strength at later ages; when the percentage of replacement exceeds 25%, it produces a systematic decrease in strength due to dilution of cement [5]. Contrary to the compressive strength reduction, additions of DPF in the range of 0.5–2% mass enhance tensile and flexural strength and their ductility, offer crack-bridging capabilities, and result in a moderate reduction in the compressive strength at high dosages [6].

Research gap and novelty. While SDA and DPF have been independently investigated, there are only a handful of studies with treated DPF used in an SDA modified matrix, which, in only a few, give age-resolved statistical characterization (mean ± standard deviation, number of replicates) and regression models with goodness-of-fit indicators [7]. The present study will focus on resolving the aforementioned issues by performing (i) the systematic evaluation of four SDA replacement levels applied to the optimum SDA matrix along with two DPF dosages, (ii) treatment of DPF in 3% NaOH solution for improving fibre-matrix bonding, (iii) testing of replicate specimens at 28, 56 and 90 days, and (iv) the generation of regression equations of (i) linear type for SDA and (ii) exponential type for DPF with related R^2 values for preliminary design [8]. Therefore, the specific objectives of the present study are:

- Experimental attempt to quantify the mechanical performance (compressive strength, splitting tensile strength, flexural strength) of concrete at ages of 28, 56 and 90 days using 0%, 5%, 10%, 20% and 30% replacements of cement with SDA, and determine the optimum dose of SDA replacement in the concrete.
- Determine the influence of incorporating 0.5% and 1% alkali-treated DPF into the optimum SDA mix and 'fiber-matrix interaction.
- Construct age-specific linear (SDA) and exponential (DPF) regression models, including R2 goodness-of-fit indicators in ranges of 0-30% SDA and 0-1% DPF, respectively.

Practical implications, limitations, and potential environmental impacts of using SDA and treated DPF as sustainable components in structural concrete should be discussed.

1.1 Literature Review

The natural reinforcement, such as date palm fiber (DPF), has been studied as reinforcement in cement-based materials such as concrete and mortar. In 2024, Said et al. [8] explored the application of natural fibres along with recycled tyre wire in cement concrete. The mixing of DPF alone increased splitting tensile strength by 127% compared to the control mix, and the combined addition of 1% DPF and 0.5% tire wire led to up to a 238% increase in tensile strength of the mixes. The compressive and flexural strengths showed a synergistic effect with increases of 121% and 171%, respectively, suggesting a strengthening effect on these properties.

AlSehali et al. [9] investigated untreated DPFs in the structural and render mortars for arid regions. The authors reported that for structural mortar, 1.5% DPF (35 mm long) and for render mortar, 0.75% DPF (10 mm long) resulted in the maximum flexural strength and an acceptable water absorption. Dehghan and Hassani. [10] conducted a study on roller-compacted concrete pavement (RCCP) reinforced with DPF and reported that flexural strength and splitting tensile strength of the reinforced RCCP increased by 11.68% and 16.83%, respectively, at 500 g/m^3 with a maximum toughness index of 1.188 at 750 g/m^3. Ozerkan et al. [11] found that the initial setting time and final setting time of the mortar were reduced up to 1% DPF and then increased at 2% DPF, but drying shrinkage was reduced up to 1% DPF, and it increased with a higher percentage of DPF. The

highest water absorption was recorded for the mix containing 0.5% DPF. Benaniba et al. [12] prepared a DPF–cement mortar composite that contained 6–30% DPF (in 6% steps) by mass, and its density, thermal conductivity, flexural strength and compressive strength were all found to decrease with increasing DPF content (except for the flexural strength, which had an initial slight increase for 6–12% DPF content).

Zanichelli et al. [13] investigated the fracture behavior of DPF-reinforced mortar ranging from 2% to 10% of fiber, increasing by 2%, and they reported that peak load, elastic modulus, and fracture toughness of the mortar decreased with increasing content of DPF. Kareche et al. [14] studied three levels of DPF additions (5%, 10%, and 15%) and found that they led to higher porosity, lower drying shrinkage (−71.4% at 15% DPF), more acid resistance, lower strength, and lower resistance to wetting and drying. Alatshan et al. [6] investigated DPF doses of 0.5, 1, 2.5%, and longer fibres of 50 mm, 60 mm, and 70 mm. Flexural strength increased with lower DPF content, while the mixes containing higher doses of DPF coupled with longer fibres had decreased flexural strengths as compared to the unreinforced control [15]. The reported advantages were that the unit weight was reduced, the energy absorption was enhanced, the thermal insulation was improved, and the impact resistance was increased.

The principal drawbacks of DPF cement composites are the reduction in compressive strength and elastic modulus due to the increase in matrix porosity, poor fiber–matrix bonding and hydroxyl attraction of fibers, which can cause swelling during mixing [16]. The surface treatment by alkali (NaOH) is also employed to remove waxes, increase surface roughness, and improve surface-to-bulk and bulk-to-interface bonding characteristics to realize the benefits of DPF [17]. In the case of SDA, Dhull. [18] partially replaced cement with SDA up to 25%, and a decrease in compressive strength with the increase in SDA content was observed, and acceptable performance was recorded up to 15% SDA content. Elinwa et al. [19] conducted an experimental investigation involving the use of up to 20% replacement of SDA by their material and concluded that slump flow of the SFM/SCC decreased as the amount of the material was increased. Elinwa and Mahmood (2002) [4] defined the pozzolanic potential of SDA and reported that the pozzolanic content (SiO_2 + Al_2O_3 + Fe_2O_3) is 73.55%, which is greater than the required pozzolanic content (70%). Majeed. [20] discussed SDAs in foamed mortar and found that optimum mechanical properties can be achieved when the replacement rate is 20%, which then deteriorated with further incrementation beyond 30%. Fahad et al. [5] prepared the eco-friendly cement D by replacing up to 20% of the conventional cement with eggshell powder and SDA. They found that the compressive strength of the cement after 28–56 days increased for up to 20% replacement, while the compressive strength of the cement decreased with an increase in the amount of SDA after 40% replacement.

The value of the present study lies in both its critical analysis and contribution. This paper presents the reviewed literature data that replacement up to 15% of SDA keeps or improves the long-term compressive strength, as the amorphous silica is able to react with calcium hydroxide formed during cement hydration to form C–S–H; and above 20- 25% of SDA replacement is detrimental. Tensile and flexural properties are always improved with a dose from 0.5% up to 1% in DPF additions, and compressive properties are comparatively less sensitive at those dose ranges. There have been few studies reporting the combined usage of alkali-treated DPF in an SDA-modified matrix as reported in the literature, and virtually no study reporting age-resolved regression equations and R^2 indicators that can be used by engineers during the initial mix design work. Furthermore, the mechanistic contribution of lignin and hemicellulose removal during NaOH treatment to fibre–matrix interfacial adhesion and long-term durability has not been quantitatively linked to age-specific mechanical data in prior combined SDA–DPF studies. The justification of the water-to-binder ratio with respect to the combined absorption behavior of SDA and DPF is also absent from the existing literature. These represent the specific research gaps addressed by the present study. Particular attention is given to this combined formulation in the present work; replicate-based statistics are reported, and predictive models of a certain range are presented and validated in that range. A detailed comparison of the present quantitative findings with each of these works in the past is provided in Section 5.

2. Experimental Program

2.1. Materials

The following are the materials used in the study.

2.1.1 Cement

The locally available Ordinary Portland cement with particular grade 43 as per IS 8112:1989 [21] was used. It was ensured that moisture did not get into the cement by keeping the bags airtight and in a dry area and were used within four weeks after manufacture to minimize moisture uptake. The physical properties of the cement tested as per IS 4031 (Parts 1, 4, 5, 6 and 11) are summarized in Table 1 and the chemical composition of the cement is presented in Table 2 obtained by X-ray fluorescence (XRF) analysis.

Table 1. Physical properties of the constituent materials

Physical property	OPC	Coarse Aggregate	Fine Aggregate
Normal consistency (%)	31	—	—
Specific gravity	3.15	2.82	2.63
Initial setting time (min)	42.5	—	—
7-day compressive strength (MPa)	21.1	—	—
Fineness modulus	—	6.85	2.62
Maximum size	75 μm	20 mm	4.75 mm
Bulk density (kg/m^3)	1441	1551	1651
Water absorption (%)	—	0.235	2.243
Crushing value (%)	—	33	—
Impact value (%)	—	24	—

Table 2. Chemical composition of OPC (mass %)

Oxide	SiO_2	Al_2O_3	Fe_2O_3	CaO	Na_2O	K_2O	MgO	TiO_2	MnO	LOI
OPC 43 (% by mass)	22.28	7.43	3.79	63.65	0.285	0.121	0.987	0.126	0.040	1.58

3.1.2 Aggregates

Fine aggregate used is local natural river sand passing the IS sieve of 4.75mm. Coarse aggregate used was crushed granite with a nominal maximum size of 20mm. The aggregates have been screened, sieved, and washed to remove dust and organic matter and have been covered and stored. All the fine aggregate was categorized as Zone II as per IS 383:2016. The physical characteristics of the aggregates are summarized in Table 3.

Table 3. Physical properties of aggregates

Property	Fine aggregate (river sand)	Coarse aggregate (crushed stone)
Maximum size	Passing 4.75 mm	20 mm
Specific gravity	2.76	2.77
Bulk density (kg/m^3)	1535.73	1630.00
Water absorption (%)	1.31	0.69
Fineness modulus	2.23	7.34
Shape/texture	Rounded, smooth	Angular, rough

2.1.3 Water

Potable tap water conforming to IS 456:2000 was used for mixing and curing of all concrete specimens. The water was free from organic contaminants and had a pH of approximately 7.0.

2.1.4 Sawdust Ash (SDA)

Sawdust was obtained from a local timber mill that primarily processed hardwood. The material was air-dried for 48 hours and incinerated in an open shallow steel pan at ambient temperature for approximately 6 hours, until complete combustion was observed (Figure 1). The resulting ash was cooled, ground in a planetary ball mill for 10 minutes, and sieved through a 600 μm IS sieve. No additional chemical treatment was applied. The preparation procedure followed established protocols [22].

Pozzolanic-reactivity justification. The chemistry of the SDA (Table 4) was measured by XRF. The total content of (SiO_2 + Al_2O_3 + Fe_2O_3) is 77.17%, which is more than the 70% minimum requirement of natural pozzolanic cement (NPC) as stipulated in ASTM C618 / IS 3812:2003, thus qualifying the SDA as a supplementary cementitious material [3]. The hydrated calcium hydroxide reacts with the amorphous silica and helps to produce more calcium silicate hydrate (C-S-H), which also refines the pores and thereby enhances the long-term strength [20].

Replacement-level selection. A search of the literature gave four values of replacement percentage by mass of the cement (5%, 10%, 20%, 30%). The point where pozzolanic enhancement is at the upper boundary of the literature and degrades the strength as controlled by dilution was identified as the optimum dosage for replacement; the boundary between the two was characterized [5]. The curing-age dependence of pozzolanic reactivity was measured on specimens tested at 28, 56, and 90 days. The specific gravity and fineness modulus of the SDA were 2.34 and 1.91 respectively. Table 5 compares these values with those reported in the literature.

Table 4. Chemical composition of SDA (mass %)

Component	SiO_2	Al_2O_3	Fe_2O_3	CaO	MgO	Na_2O	K_2O	Loss on ignition	Combined SiO_2 + Al_2O_3 + Fe_2O_3
Mass %	62.87	9.85	4.45	10.35	4.18	0.035	1.17	5.85	77.17

Table 5. Physical properties of SDA compared with literature

Property	Present study	Ettu et al. [30] 2013	Raheem et al. [31] 2012	Mageswari et al. [33] 2009
Specific gravity	2.34	2.05	2.19	2.15
Fineness modulus	1.91	1.89	—	1.78

(a) Raw sawdust (b) Open-air combustion (c) Resulting sawdust ash

Fig. 1. Sequential conversion of sawdust-to-sawdust ash

2.1.5 Date Palm Fibre (DPF)

The fibres from the waste of the leaf stalk of date palm trees were obtained. The fibres were soaked in water for 24 hours to soften the bundles, afterwards carefully combed and cut down to the lengths of 20-30 mm and width of 0.2-1.0 mm, and then air dried for 48 hours at the ambient condition [8]. Alkali treatment. The fibres were treated with 3% (w/w) NaOH solution at room temperature (23 ± 2 °C) for 3 hours with a fibre-to-solution ratio of 1:30, and the waxes, lignin, and hemicellulose were removed, while the surface of the fibres was roughened, thus making them more suitable for interfacial bonding. Mechanistically, NaOH hydrolyses the ester bonds in hemicellulose and partially dissolves the amorphous lignin matrix, exposing the crystalline cellulose microfibrils and increasing surface roughness. This depolymerization of the hydrophilic surface layer reduces moisture-induced swelling of the fibres during mixing, and the increased surface area and roughness promote mechanical interlock and chemical adhesion with the cement paste, thereby improving the interfacial transition zone (ITZ) strength and long-term fibre–matrix bonding durability [17]. The use of 3% NaOH & 3 h immersion is based on Ali-Boucetta et al. [17] & Adamu et al., who have concluded that 3% NaOH at 3 h immersion is the minimum necessary to remove the surface waxes without causing the degradation of fibres. The fibres were then rinsed several times with deionized water till the rinse pH was detected to be 7.0 ± 0.2 after using a calibrated pH meter, indicating neutrality of the fibres. The fibres were then air-dried for 48 hours and followed by oven drying for 24 hours at 60 °C until a constant weight was achieved.

The alkali treatment would be expected to cause surface roughness of the fibre (this was qualitatively confirmed by visual inspection of the treated fibre and untreated fibre in Figure 2), to cause the removal of the hydrophilic surface layer, and to better bond the fibre to the cementitious matrix. Section 5.2 reports these improvements in tensile and flexural properties.
The treated fibres were added at 0.5% and 1% by mass of binder to mixes containing the optimum 5% SDA. The physical properties of treated DPF are summarized in Table 6.

Table 6. Physical properties of treated DPF

Property	Range
Bulk density (kg/m^3)	512.2–1088.8
True density (kg/m^3)	1300.0–1450.0
Natural moisture content (%)	9.5–10.5
Water absorption after 5 min (%)	60.1–84.1
Water absorption at saturation (%)	96.8–202.0

(a) Untreated DPF (interwoven) (b)Alkali-treated separated fibres

Fig. 2. Untreated and alkali-treated date palm fibres

2.2. Mix Design and Proportions

The concrete mixes were proportioned to the absolute-volume method as specified in IS 10262:2019 and IS 8112:1989 [21] with the initial ratio (1: 1.5: 3) and a constant water-binder ratio (w/b) of 0.45 for all the mixes. The w/b ratio of 0.45 was selected on the basis of the combined

water demand of the SDA and DPF. SDA, with a higher specific surface area than OPC, increases paste viscosity and water demand at elevated replacement levels [19]; however, at the optimum 5% SDA dose used in the fibre mixes, this effect is minor. The high-water absorption of DPF (60.1–202% at saturation, Table 6) was managed by pre-soaking the fibres to a saturated surface-dry condition before mixing, consistent with the SSD correction protocol applied to the aggregates, so that the effective w/b ratio remained 0.45 across all mixes. This ensured workability consistency and direct comparability among all mix groups. In the control mix, 436 kg/m^3 of OPC, 655 kg/m^3 of fine aggregate, 1309 kg/m^3 of Coarse aggregate, and 196 kg/m^3 of water were used. All of the SDA mixes had a constant water demand, so that they could be directly compared, and the workability of each of these mixes was monitored using slump, and the results are reported in Section 4.1. The full mix design for all seven mixes investigated (including the three DPF mixes) is summarized in Table 7.

Table 7. Mix design proportions of all concrete mixes investigated (per m^3)

Constituent	PC (control)	H5%	H10%	H20%	H30%	DPF0.5%	DPF1%
OPC (kg/m^3)	436	414.2	392.4	348.8	305.2	414.2	414.2
SDA (kg/m^3)	0	21.8	43.6	87.2	130.8	21.8	21.8
Treated DPF (kg/m^3)	0	0	0	0	0	2.18	4.36
Fine aggregate (kg/m^3)	655	655	655	655	655	655	655
Coarse aggregate (kg/m^3)	1309	1309	1309	1309	1309	1309	1309
Water (kg/m^3)	196	196	196	196	196	196	196
w/b ratio	0.45	0.45	0.45	0.45	0.45	0.45	0.45
Specimens per age*	9	9	9	9	9	9	9

Note: 9 specimens per age = 3 cubes (compressive) + 3 cylinders (tensile) + 3 prisms (flexural); total per mix = 27 specimens across the 3 curing ages.

2.3. Sample Preparation

The mixing was done in a laboratory pan-type concrete mixer (100L capacity) with a rotation speed of 36 rpm. Aggregates were used in the saturated surface-dry (SSD) condition, and corrections have been made for water absorption, as shown in Tables 1 and 3. A strict homogeneity was demanded in the mixing sequence:

- Cement, SDA (where applicable), and fine aggregate were dry-mixed for 60 s in the pan mixer to disperse SDA and avoid lumps.
- Coarse aggregate was added and dry-mixed for a further 60 s.
- Pre-treated DPF (where applicable) was hand-sprinkled gradually during the dry mix to avoid balling. At this stage, it was visually checked for even dispersion of fibres before adding water.
- Water was added in two stages (60% then 40%) with continuous mixing for 180 s after water addition. The total mixing time was about 5 min.
- The slump was measured immediately, according to IS 1199:1959, and the results are presented in Section 4.1.
- The fresh concrete was cast in steel moulds in three layers, each compacted on a vibrating table for 15 s. Specimen sizes were 150 × 150 × 150 mm cubes (compressive), 150 mm diameter × 300 mm height cylinders (splitting tensile), and 100 × 100 × 500 mm prisms (flexural).

- Damp hessian was placed over the specimens for 24 h in the laboratory at 23 ± 2 °C, followed by transfer to a water-curing tank at 23 ± 2 °C and relative humidity ≥ 95%.
- Three replicate specimens per mix per age per test were prepared, giving 27 specimens per mix and 189 specimens for the seven mixes.

(a) Mixing

(b) Casting

(c) Water curing

(d) Compressive test

(e) Splitting tensile test

(f) Flexural test

Fig. 3. Experimental setup: (a) mixing, (b) casting, (c) curing, and (d–f) mechanical testing

2.4. Testing Methods

All mechanical tests were performed at 28, 56, and 90 days. Three replicates were tested for each mix at each age, and means and standard deviations were reported in Section 5. Specimens were tested in the SSD condition. All failure modes were documented on each specimen, and the standard deviation (SD) and coefficient of variation (CV) were used to determine the dispersion.

2.4.1 Compressive Strength

The cube compressive strength was evaluated as per IS 516:2018 Part-1 Section-1 with a 2000 kN compression testing machine with a loading rate of 0.2 ± 0.02 MPa/s. A load was placed between the platens of the cubes centrally without shocks until failure occurred. The compressive strength was determined as shown above:

$$\sigma = \frac{P}{A} \tag{1}$$

Where σ is the compressive strength (MPa), P is the maximum load (N) and A is the cross-sectional area (mm^2).

2.4.2 Splitting Tensile Strength

The splitting tensile strength was evaluated based on IS 5816:1999 using a cylindrical specimen (150 mm diameter x 300 mm height). These cylinders were set up horizontally in hardboard packing, and loading was done at a rate of 1.2-2.4 MPa per minute until failure occurred. The splitting tensile strength was measured at:

$$ft = \frac{2P}{\pi LD} \tag{2}$$

Where ft is the splitting tensile strength (MPa), P is the failure load (N), L is the specimen length (mm) and D is the specimen diameter (mm).

3.4.3 Flexural Strength

The flexural strength followed IS 516:1959 (reaffirmed 2018) on test specimen, prism of size 100 × 100 × 500 mm with clear span of 400 mm at a loading rate of 0.7 MPa/min. It was calculated that:

$$fb = \frac{PL}{bd^2} \quad (3)$$

Where fb is the flexural strength (MPa), P is the failure load (N), L is the support span (mm), b is the average width (mm) and d is the average depth (mm).

2.4.4 Statistical Analysis

Mean of the replicate measurements (μ), standard deviation of the replicate measurements (σ), and coefficient of variation (CV = σ/μ) were calculated for each property based on three reps per mix per age. For all the means reported with error bars in bar charts and with a standard deviation in Tables 8 and 9, the standard deviation is indicated by an error bar next to each mean. Only 5.2% of the maximum CV was achieved in this study, which is acceptable when considering replicate consistency. Age-resolved trends and the relative effects of SDA and DPF were further analyzed by linear (SDA) and exponential (DPF) regression with R^2 given as an indicator of goodness-of-fit.

2.4.5 Parametric Modelling Framework

A multiple regression analysis was done at each curing time. For SDA-only mixes (V_fs between 0 and 30), ordinary least squares were used to fit a linear model y = a − b·V_fs as the trend with SDA was shown to be monotonic and approximately linear after the small (5%) pozzolanic peak, consistent with the dilution-dominated regime reported in [5]. The exponential model y = a·exp(b·x) was found suitable for 5% SDA (dosage x ranging from 0.5% to 1.0%) due to the known strong non-linearity in crack-bridging effect of fibres in concrete reinforcement (particularly in tension and bending), y (tensile and flexural strength, respectively) [24]. Both models can only be applied in the experimental range: V_fs is between 0 and 30%, and x is between 0,5% and 1,0%, only extrapolation within the range is recommended. The selection of a linear model for SDA was justified by the approximately monotonic, dilution-dominated decrease in strength above 5% SDA, which is consistent with previously reported linear trends in the literature [20], and by the absence of a pronounced inflection point that would warrant a more complex nonlinear formulation. Higher-order polynomial or power-law models were tested but did not yield significantly improved R^2 values for the present five-point dataset. The exponential model for DPF was chosen because of the known strong non-linearity in the crack-bridging response of fibres in concrete, particularly in tension and bending; the exponential form provides a better fit than a linear model to data that show an accelerating increase in strength with dosage over a limited range. With only three data points per age (0%, 0.5%, 1% DPF), R^2 = 1.00 is a geometric necessity for two-parameter curve fitting, and these DPF models should be interpreted strictly as interpolation tools within the tested dosage range rather than validated predictive equations.

3. Workability and Mix Verification

3.1. Slump Test Results

The slump test (IS 1199:1959) was used to assess the fresh-state workability of all seven mixes immediately after mixing, and the results were summarized in Table 8. As the SDA content was increased, the slump dropped gradually from 78 mm for the control mix to 38 mm at 30% SDA. A higher fineness and water requirement of SDA particles than that of cement has caused this trend, as stated by Elinwa et al. [19]. Improvements in slump were realized with the addition of 0.5% and 1% DPF to the 5% SDA mix (Table 6), which is due to the high-water absorption capacity of the fibers. The addition of 0.5% and 1% DPF to the 5% SDA mixes further reduced workability (Table 8), attributable to the high-water absorption capacity of the fibres, which reduces the effective water available for lubrication of the fresh mix. All mixes were suitable, and the slump was kept within a compatible range with no use of superplasticizer; however, for any applications requiring a high slump (self-compacting concrete), it is recommended that a polycarboxylate type admixture be used.

Table 8. Slump test results of all mixes

Mix	Slump (mm)	Workability classification (IS 456)
PC (control)	78	Medium
H5%	72	Medium
H10%	65	Medium
H20%	48	Low
H30%	38	Low
5% SDA + 0.5% DPF	62	Medium
5% SDA + 1% DPF	51	Low

4. Experimental Results and Discussion

This section reports the mechanical performance of SDA-modified concrete (Section 5.1) and of DPF-reinforced concrete with the optimum SDA content (Section 5.2). All strength values are reported as the mean ± standard deviation of three replicates. Regression equations include R^2 as a goodness-of-fit indicator.

4.1. Mechanical Properties of SDA Concrete

Table 9 shows the compressive strength, splitting tensile strength, and flexural strength of the five SDA mixes (0%, 5%, 10%, 20%, and 30%) at 28, 56, and 90 days. Mean (SD) was followed by standard deviation. Replicate consistency was good, as the reported coefficient of variation was never more than 5.2%.

Table 9. Mean (± SD) mechanical strengths of SDA concrete at 28, 56 and 90 days (n = 3)

Mix	Comp. 28d	Tens. 28d	Flex. 28d	Comp. 56d	Tens. 56d	Flex. 56d	Comp. 90d	Tens. 90d	Flex. 90d
H0	38.74 (±0.62)	5.03 (±0.11)	4.47 (±0.09)	42.15 (±0.71)	5.29 (±0.14)	4.89 (±0.13)	43.67 (±0.85)	5.43 (±0.12)	5.17 (±0.14)
H5%	38.91 (±0.59)	5.12 (±0.10)	4.81 (±0.12)	44.67 (±0.83)	5.53 (±0.15)	5.23 (±0.14)	45.43 (±0.77)	5.84 (±0.15)	5.65 (±0.16)
H10%	38.18 (±0.71)	4.47 (±0.13)	4.36 (±0.11)	43.17 (±0.78)	5.32 (±0.14)	4.94 (±0.15)	44.16 (±0.92)	5.68 (±0.16)	5.23 (±0.15)
H20%	26.42 (±0.74)	3.54 (±0.16)	3.41 (±0.12)	29.51 (±0.81)	3.81 (±0.15)	3.65 (±0.13)	31.11 (±0.95)	3.91 (±0.15)	3.71 (±0.14)
H30%	21.69 (±1.05)	2.93 (±0.15)	2.28 (±0.14)	23.57 (±1.12)	3.00 (±0.16)	2.41 (±0.13)	25.72 (±1.22)	3.17 (±0.16)	2.49 (±0.15)

Note: All strength values are in MPa. Standard deviation in parentheses (n = 3).

4.1.1 Effect of SDA on Compressive Strength

The compressive strength of the cube with varying SDA replacement percentages is plotted in Figures 5 and 6. With 5% SDA, the 28-, 56-, and 90-day compressive strengths were essentially the same or slightly greater than the control (+0.4%, +6.0%, and +4.0%, respectively). It is in line with the pozzolanic reaction of amorphous silica with $Ca(OH)_2$ generated by the cement hydration process, which leads to further production of C–S–H and smooths the pores in the matrix [19][3].

Again, it was observed that there was a small reduction at 10% SDA (-1.4%) at 28 days with a partial recovery at later ages (+2.4% at 56 days and +1.1% at 90 days). The compressive strength for cement decreases with increasing concentration; above 20% SDA, the cement becomes more dilute, leading to decreases in 28-day and 90-day compressive strength equal to 31.8% and 44.0%, respectively. This is in line with the reported work by Raheem et al. [23] that observed that a drop in mechanical performance is observed at 25% SDA and after 90 days, while Majeed [20] observed mechanical performance reducing at the same threshold (≈20%) with days exceeding 90.

(a) Specimen identification (b) Specimen at failure (c) Failure mode

Fig. 4. Cube compressive strength test of SDA specimens

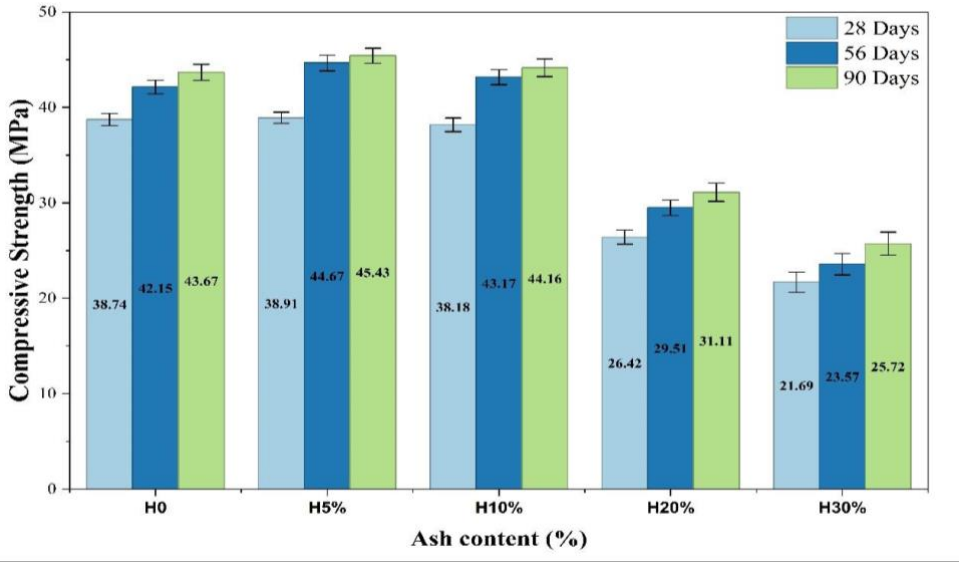

Fig. 5. Cube compressive strength test of SDA specimens

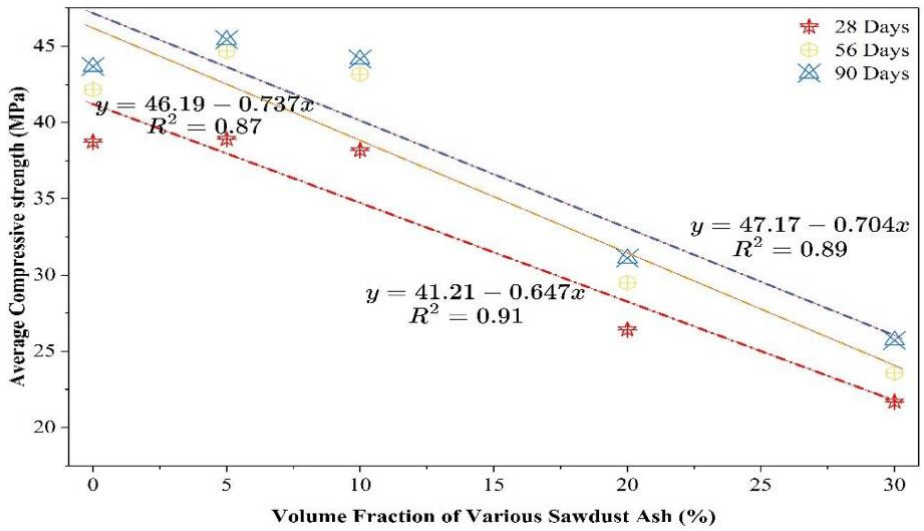

Fig. 6. Linear regression of compressive strength versus SDA content

The variation of compressive strength with SDA volume fraction at each age (Figure 6) was well represented by linear regression. The fitted equations and R^2 values are:

$$fcs = 41.21 - 0.647Vfs \quad (4)$$

$$fcs = 46.19 - 0.737Vfs \quad (5)$$

$$fcs = 47.17 - 0.704Vfs \quad (6)$$

The relationship between ASTM (cube strength, MPa) and the SDA replacement level (percentage by mass of cement) is shown as High R^2 values (0.87-0.91) verify the existence of a linear relation between 0% and 30% SDA. The magnitude of the slope is also consistent with those reported elsewhere in the literature, with the Raheem et al. [23] study reporting a slope of approximately −0.65 MPa per % SDA at 28 days of incubation, comparing favorably with the slope of Eq. (4). These equations (4), (5), and (6) can thus be applied as preliminary design tools in limiting ranges of replacement percentages of 0 to 30% and curing periods of 28 to 90 days for SDA concrete structures.

4.1.2 Effect of SDA on Splitting Tensile Strength

The splitting tensile strengths (Figures 8–9) followed a trend qualitatively similar to the compressive strength. At 5% SDA, tensile strength improved by 1.8%, 4.5%, and 7.5% at 28, 56, and 90 days relative to control, attributable to the pozzolanic C–S–H formation that reduces matrix microporosity. At 10% SDA, the 28-day tensile strength was 11.1% lower than the control but partially recovered to +0.6% at 56 days and +4.6% at 90 days. Beyond 20% SDA, the loss became substantial (−29.6% at 20% and −41.7% at 30%, at 28 days).

(a) Specimens (b) Loading setup (c) Failure pattern

Fig. 7. Splitting tensile strength test of SDA specimens

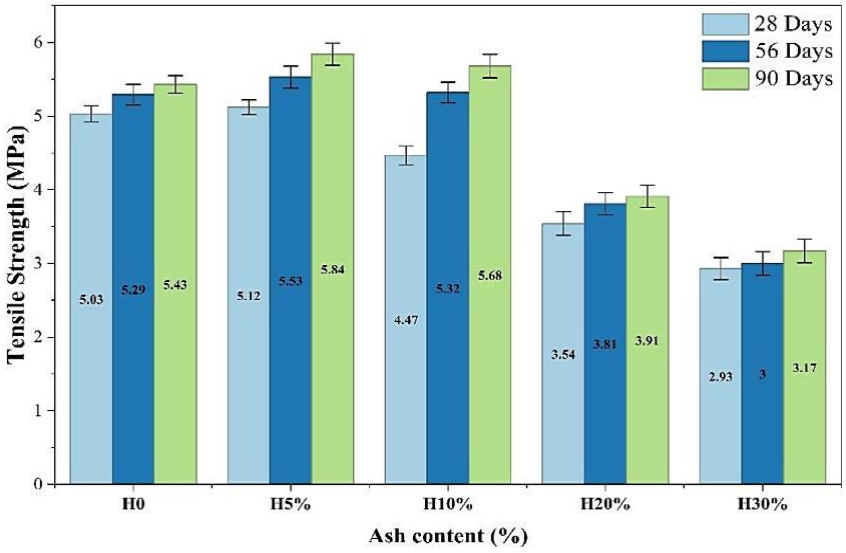

Fig. 8. Splitting tensile strength of SDA concrete at 28, 56 and 90 days (mean ± SD)

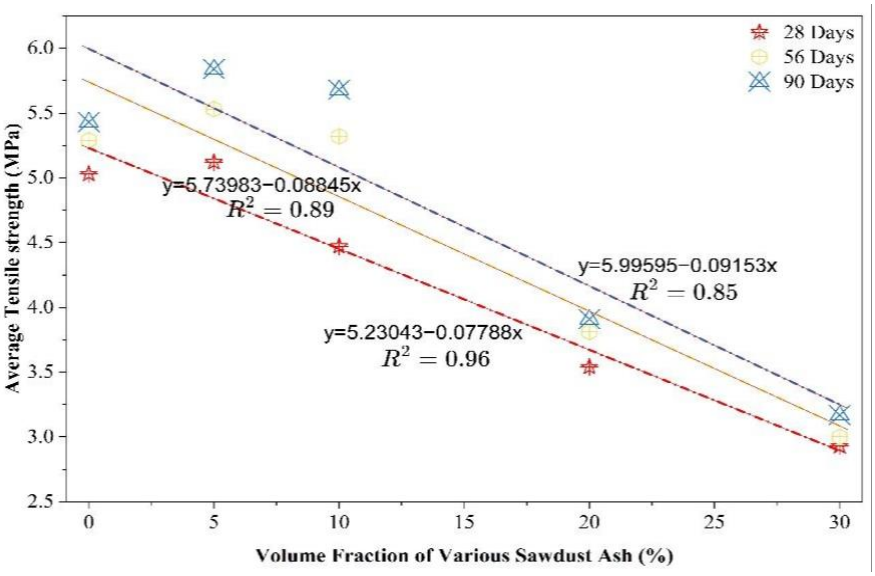

Fig. 9. Linear regression of splitting tensile strength versus SDA content

The linear regression equations for splitting tensile strength against SDA volume fraction are:

$$fts = 5.230 - 0.0778Vfs \quad (7)$$

$$fts = 5.739 - 0.0884Vfs \quad (8)$$

$$fts = 5.995 - 0.0915Vfs \quad (9)$$

Where fts is the splitting tensile strength (MPa). The lowest correlation, 96% on day 28, confirms the almost linear dilution-controlled trend at the earliest age, while the reduction in R^2 with curing age indicates the small non-linearities around the 10% SDA point, which is caused by the gradual pozzolanic recoveries with curing age.

4.1.3 Effect of SDA on Flexural Strength

The flexural strengths (Figures 11-12) at 5% SDA were higher than the control at 28, 56, and 90 days, respectively, with the highest relative difference of 9.3% for the 90-day strength level. At 10% SDA, a slight 2.5% reduction at 28 days was followed by 1.0% and 1.2% improvements at 56 and 90 days. For flexural strength, both 20% and 30% SDA resulted in a 23.7–28.2% and 49–52% decrease, respectively, in the three ages. These decreases are due to lower cement levels and higher matrix porosities at high SDA doses. The linear regression equations for flexural strength are:

$$ffs = 4.920 - 0.0811Vfs \quad (10)$$

$$ffs = 5.428 - 0.0926Vfs \quad (11)$$

$$ffs = 5.790 - 0.1031Vfs \quad (12)$$

where ffs is the flexural strength (MPa). The trend is consistent with Marthong [25] and Dhull [18].

Optimum SDA content. Overall, the strength performance at 5% SDA (compressive 45.43 MPa, tensile 5.84 MPa, flexural 5.65 MPa at 90 days) was found to be similar to or slightly higher than that of the control, in all three strength tests and at all ages. At greater than 10% SDA, the cement dilution effect was significant. The 5% SDA replacement is, therefore, chosen as the optimum and treated as the matrix for the mixes formulated with DPF replacements in Section 5.2.

(a) Prism specimens (b) Loading (c) Failure

Fig. 10. Flexural strength test of SDA specimens

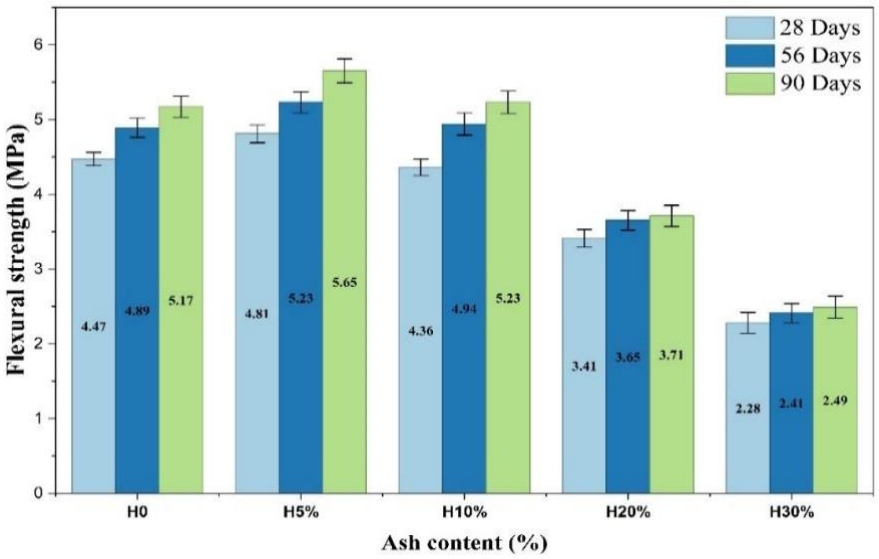

Fig. 11. Flexural strength of SDA concrete at 28, 56 and 90 days (mean ± SD)

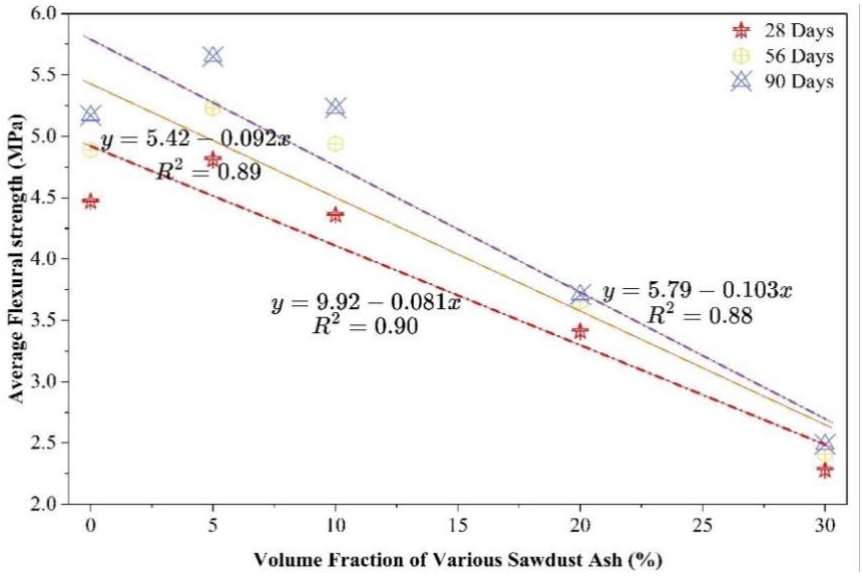

Fig. 12. Linear regression of flexural strength versus SDA content

4.2 Mechanical Properties of DPF Concrete with Optimum SDA

Table 10. summaries the strengths of the three mixes containing 5% SDA with 0%, 0.5%, and 1% treated DPF. All values are the mean of three replicates with the standard deviation in parentheses.

Table 10. Mean (± SD) mechanical strengths of DPF concrete (with 5% SDA) at 28, 56 and 90 days (n = 3)

Mix	Comp 28d	Tens. 28d	Flex. 28d	Comp. 56d	Tens. 56d	Flex. 56d	Comp. 90d	Tens. 90d	Flex. 90d
H5% (ref)	38.91 (±0.59)	5.12 (±0.10)	4.81 (±0.12)	44.67 (±0.83)	5.53 (±0.15)	5.23 (±0.14)	45.43 (±0.77)	5.84 (±0.15)	5.65 (±0.16)
DPF 0.5%	39.43 (±0.61)	6.12 (±0.13)	7.34 (±0.18)	45.32 (±0.79)	6.53 (±0.16)	7.89 (±0.21)	46.21 (±0.84)	6.82 (±0.17)	8.22 (±0.23)
DPF 1%	40.23 (±0.72)	7.23 (±0.16)	9.17 (±0.24)	46.11 (±0.86)	7.51 (±0.18)	9.79 (±0.26)	46.89 (±0.89)	7.92 (±0.19)	10.24 (±0.27)

Note: All strength values are in MPa. Standard deviation in parentheses (n = 3).

4.2.1 Effect of DPF on Compressive Strength

The compressive strengths (Figures 14–15) increased only modestly with DPF addition: at 0.5% DPF, gains over the 5% SDA reference were 1.3%, 1.5%, and 1.7% at 28, 56, and 90 days, respectively; at 1% DPF, the corresponding gains were 3.4%, 3.2%, and 3.2%. Modest compressive gains are typical of natural-fibre reinforced concrete: fibres do not significantly enhance the matrix compressive strength but bridge microcracks and delay coalescence into a macrocrack [24]. The small magnitude of improvement is also consistent with Yasser et al. [24] and with Said et al. [8].

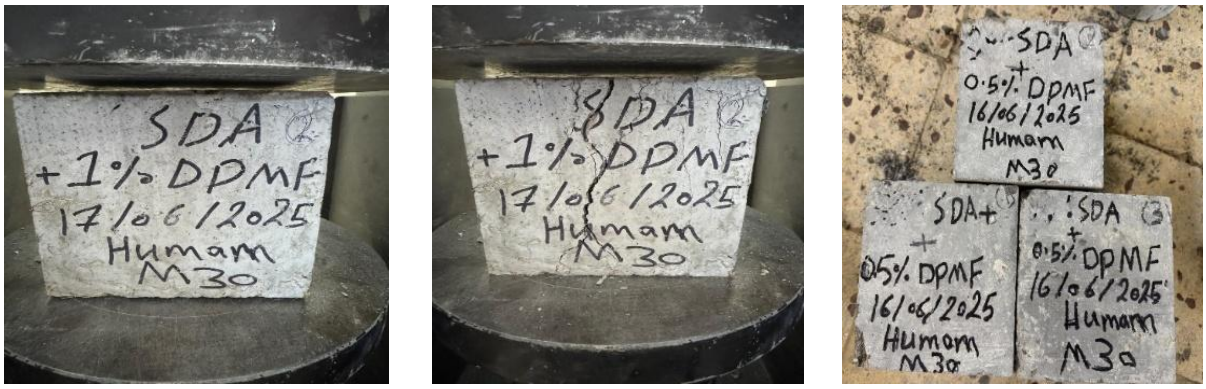

(a) DPF concrete cube (b) Loading (c) Failure

Fig. 13. Compressive strength test of DPF specimens (with 5% SDA)

The exponential regression equations are:

$$fcd = 38.64e^{0.040x} \qquad R^2=1.00 \tag{13}$$

$$fcd = 44.54e^{0.034x} \qquad R^2=1.00 \tag{14}$$

$$fcd = 45.54e^{0.029x} \qquad R^2=1.00 \tag{15}$$

where x is the DPF dosage (% by mass of binder). Note that with only two non-zero data points per age (0.5% and 1.0% DPF), R^2 is necessarily 1.00; the equations should be regarded as interpolation tools within the dosage range $x \in [0.5\%, 1.0\%]$ and should not be extrapolated outside this range.

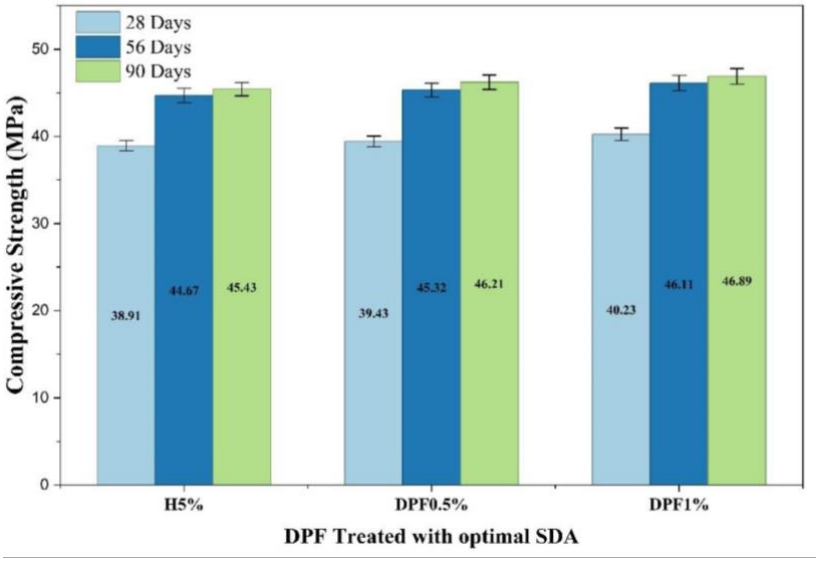

Fig. 14. Compressive strength of DPF concrete versus reference (5% SDA)

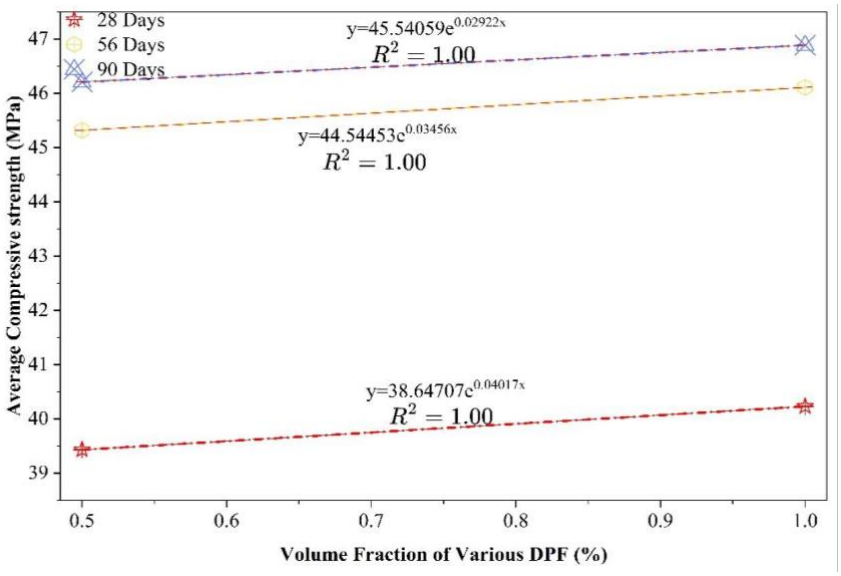

Fig. 15. Exponential regression of compressive strength versus DPF content

4.2.2 Effect of DPF on Splitting Tensile Strength

The splitting tensile strengths (Figures 17–18) increased substantially with DPF: 0.5% DPF gave 19.5%, 23.4%, and 25.6% increases at 28, 56, and 90 days, respectively, while 1% DPF gave 41.2%, 42.0% and 45.9%. The improvement reflects the crack-bridging action of the fibres, which transfer tensile stress across cracks and delay their propagation. Under tensile loading, alkali-treated DPF promotes microcrack bridging at the onset of cracking: the fibres bridge the crack flanks, transferring load through a combination of frictional pull-out resistance and chemical bonding at the improved ITZ, thereby resisting crack propagation and increasing the energy required for crack coalescence into a macrocrack. This post-cracking mechanism explains the marked gains in splitting tensile strength relative to the modest compressive gains, since the crack-bridging mechanism is activated primarily under tensile stress states. Variability in tensile response (CV up to 5.2%) is partly attributable to random fibre orientation and localized clustering; future work using controlled fibre alignment or optimized dispersion protocols could reduce this variability and further improve structural reliability. Alkali treatment of the fibres further enhances bonding with the matrix, as supported by Ali-Boucetta et al. [17].

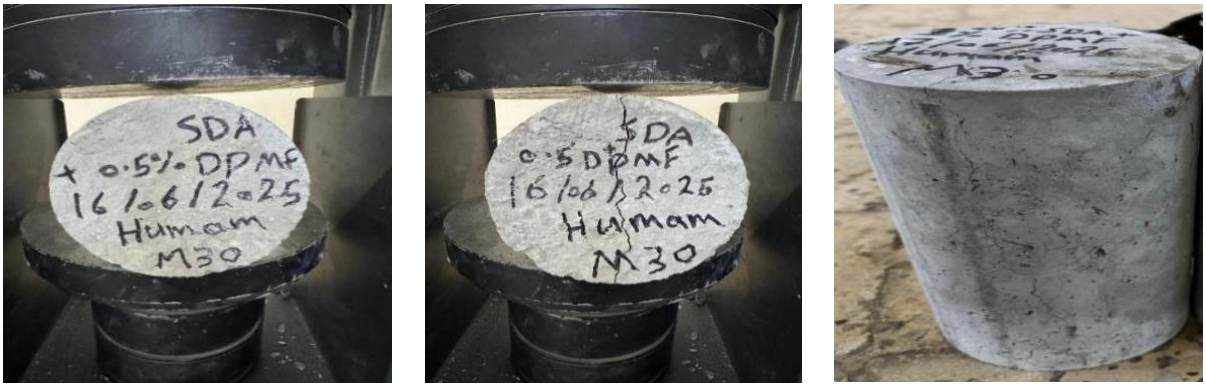

(a) Specimens (b) Loading (c) Failure crack

Fig. 16. Splitting tensile strength test of DPF specimens (with 5% SDA)

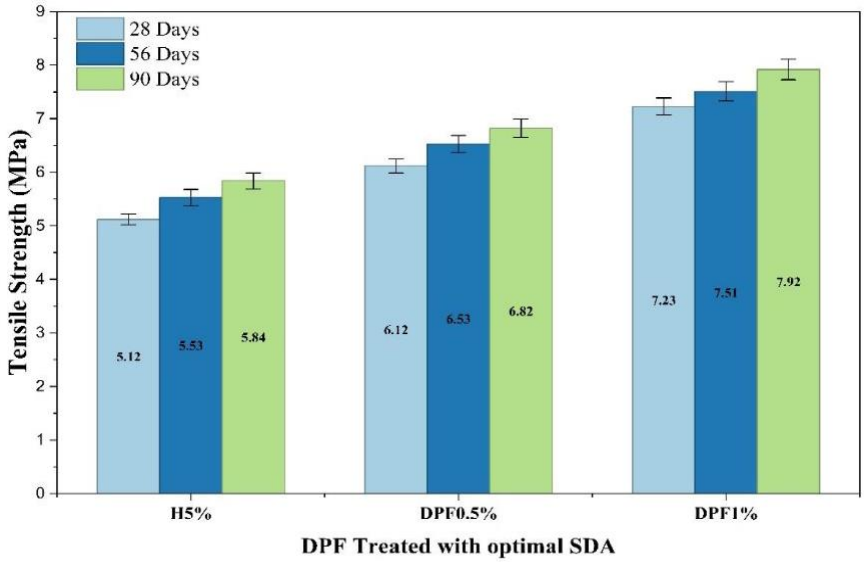

Fig. 17. Splitting tensile strength of DPF concrete versus reference (5% SDA)

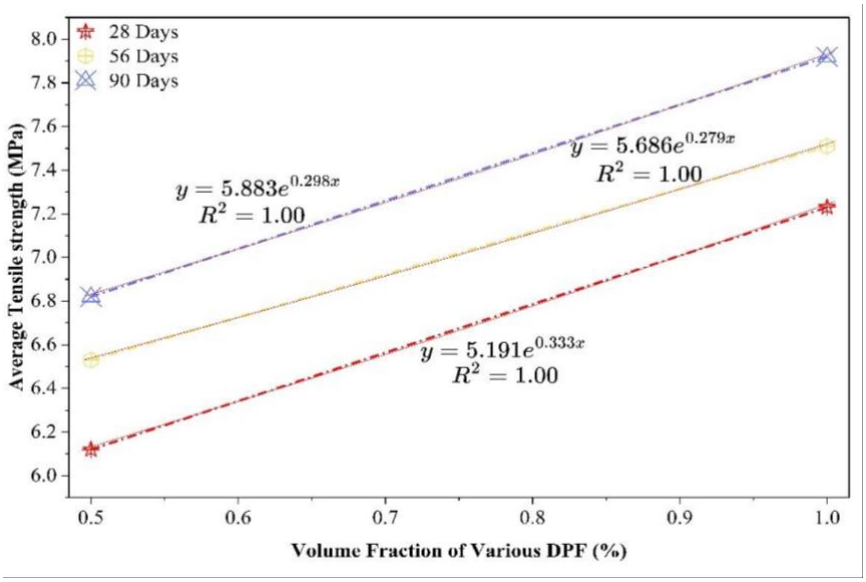

Fig. 18. Exponential regression of splitting tensile strength versus DPF content

The exponential regression equations are:

$$ftd = 5.191e^{0.333x} \qquad R^2=1.00 \tag{16}$$

$$ftd = 5.686e^{0.279x} \qquad R^2=1.00 \tag{17}$$

$$ftd = 5.883e^{0.298x} \qquad R^2=1.00 \tag{18}$$

4.2.3 Effect of DPF on Flexural Strength

Flexural strength (Figures 20–21) showed the most pronounced improvement: 0.5% DPF gave increases of 62.0%, 67.5%, and 69.1% increases at 28, 56, and 90 days, respectively, while 1% DPF gave 103%, 108%, and 111%. Flexural strength is most sensitive to fibre reinforcement because the failure of unreinforced concrete in flexure occurs by tensile cracking at the soffit, where fibres are most effective at bridging cracks and prolonging the post-peak load. This is consistent with the findings of Benaimeche et al. [26], who reported similar magnitudes of flexural gain in alkali-treated DPF mortar, and with the lower compressive strength gains observed in Section 5.2.1, which is the expected hierarchy for fibre-reinforced cement composites.

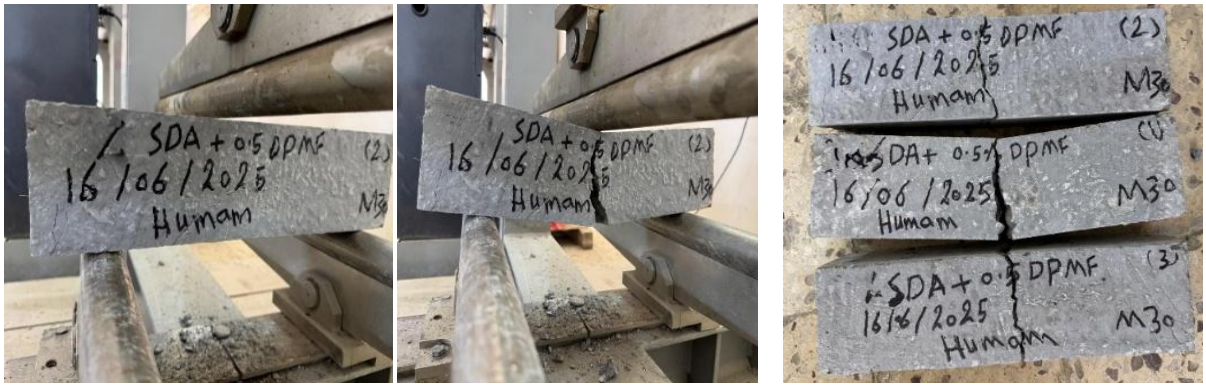

(a) Prism specimens (b) Loading (c) Crack bridging at failure

Fig. 19. Flexural strength test of DPF specimens (with 5% SDA)

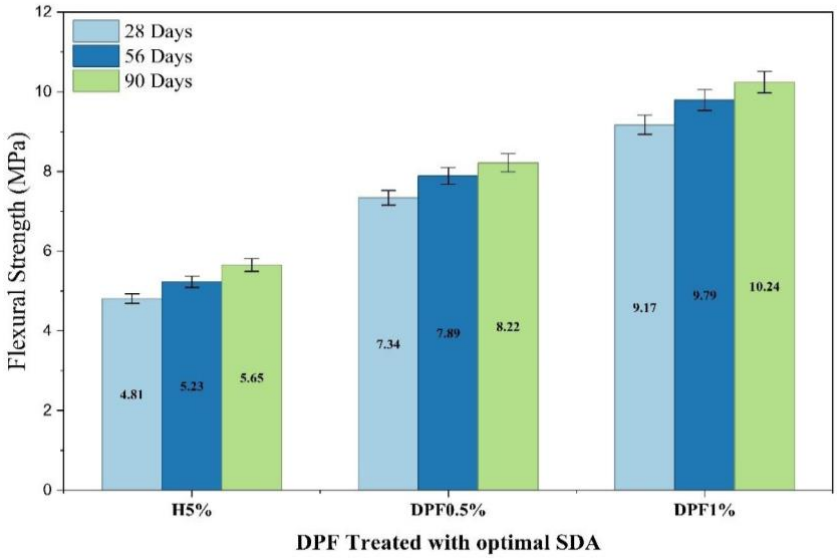

Fig. 20. Flexural strength of DPF concrete versus reference (5% SDA)

The exponential regression equations are:

$$frd = 5.899e^{0.444x} \qquad R^2 = 1.00 \tag{19}$$

$$frd = 6.383e^{0.431x} \qquad R^2 = 1.00 \tag{20}$$

$$frd = 6.624e^{0.438x} \qquad R^2 = 1.00 \tag{21}$$

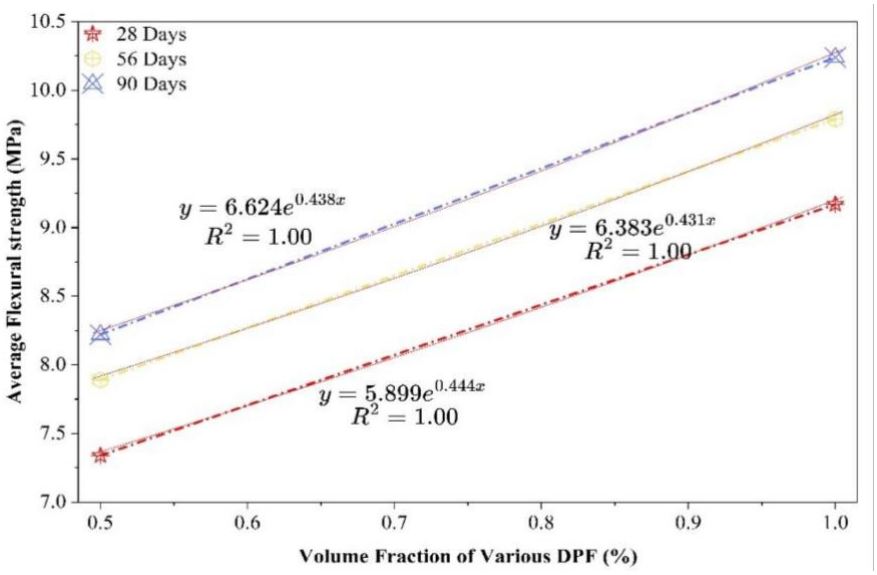

Fig. 21. Flexural strength of DPF concrete versus reference (5% SDA)

4.3 Comparative Analysis with Previous Studies

Table 11 compares the present results with some recent studies. The compressive-strength loss at 25–30% SDA reported here (−44% at 30% SDA, 90 days) is consistent with Raheem et al. [23] (−36% at 25% SDA), Marthong [25] (−40% at 20% SDA), and Majeed [20] (−45% at 30% SDA in foamed mortar). For DPF, the present tensile gains at 1% DPF (≈41–46%) lie between Alatshan et al. [6] (≈30% at 1% DPF) and Said et al. [8] (≈127% at 1% DPF with hybrid tyre wire). The flexural strength increases of ≈100–110% at 1% DPF is amongst the highest reported, which is greater than that reported by Benaimeche et al. [26], which amounted to ≈70% at a similar dosage. This improvement is likely attributable to 3% NaOH fibre treatment used in the present study.

Table 11. Comparison of present results with recent literature

Reference	Material	Replacement / Dosage	Property	Change vs. control
Present study	SDA (alone)	5% / 30%	Compressive @ 90 d	+4.0% / −41.1%
Raheem et al. [23]	SDA	25%	Compressive @ 90 d	−36%
Majeed [20]	SDA in foamed mortar	30%	Compressive @ 28 d	−45%
Fahad et al. [5]	ESP + SDA	20%	Compressive @ 28 d	+29.6%
Present study	DPF (with 5% SDA)	1%	Tensile @ 90 d	+45.9%
Alatshan et al. [6]	DPF	1% (60 mm)	Tensile	≈+30%
Said et al. [8]	DPF + tyre wire	1% + 0.5%	Tensile	+238%
Present study	DPF (with 5% SDA)	1%	Flexural @ 90 d	+111%
Benaimeche et al. [26]	DPF in mortar	1%	Flexural	≈+70%

4.4 Microstructural Interpretation and Hydration Mechanism

The direct microscopic (SEM/EDS) imaging of the present specimens is not within the scope of this experimental phase and is identified as a limitation, but the macroscopic tendencies reported above are consistent with hydration mechanisms reported in the SDA and DPF literature [17]. With SDA contents ≤5%, the amorphous silica reacts with the $Ca(OH)_2$ formed during the hydration of C_3S and C_2S to produce further C–S–H that refines the pore structure and produce the steady strength gain between 28 and 90 days as detailed in Table 9. This pozzolanic reaction progressively consumes calcium hydroxide (CH), converting a relatively weak and soluble phase into additional C–S–H gel that densifies the capillary pore network and reduces porosity. The age-dependent

consumption of CH during long-term hydration (28 to 90 days) is consistent with the progressive strength gain observed for the 5% SDA mix and explains the small non-linearity in the regression trends at later ages. All microstructural interpretations in this section are presented as plausible, literature-supported mechanisms; they are not directly demonstrated and await confirmation by SEM/EDS/MIP analysis in dedicated future work. When SDA contents are high (≥20%), the lower amount of cement clinker leads to insufficient quantities of Ca $(OH)_2$ for reaction and an increase in unreacted silica, which leads to matrix dilution and a reduction in strength. For concrete reinforced with DPF, the surface of the DPF is treated with alkali, making it rougher and less waxy, which in turn provides better mechanical interlock with the matrix, resulting in greater tensile and flexural strength. Future work on SEM/EDS/MIP is noted as a dedicated study to give microscopy proof of the formation of the C–S–H, refinement of pores and fibre–matrix interface.

4.5 Sustainability Considerations and Limitations

The 5% reduction in OPC reduces the cement-related CO_2 emissions by an estimated 5%. OPC clinker production is the dominant source of emissions, accounting for approximately 900 kg CO_2-eq per ton of clinker. Based on this assumption, the cement saving of approximately 21.8 kg per m^3 (at 5% SDA) corresponds to a preliminary estimate of approximately 20 kg CO_2-eq per m^3, this figure is an assumption-based approximation and does not constitute a full life-cycle assessment (LCA). The valorization of DPF, which would otherwise be open-burned in many date-producing regions, also contributes additional environmental benefits. A comprehensive LCA including transportation, fibre treatment, energy, and end-of-life scenarios is identified as an important area for future work. Similarly, although mechanical performance has been investigated in this work, other important properties of long-term durability (chloride and sulphate resistance, freeze-thaw, carbonation, alkali–fibre stability, degradation of cellulose fibres in alkaline pore solution) remain to be evaluated and are noted as important areas for future research prior to the deployment of the structure. From a waste management perspective, the concurrent utilization of SDA and DPF in concrete diverts two categories of agro-industrial residue from landfill or open burning. Sawdust, generated in large quantities by the timber and furniture industry, is commonly disposed of by open combustion or landfilling; its conversion to SDA and use as a supplementary cementitious material represents a valorization pathway that reduces solid waste volume. Similarly, date palm rachis fibres are typically open-burnt after pruning in date-producing regions, releasing particulate matter and CO_2; their utilization as fibre reinforcement reduces this open-burning burden. Together, these two waste streams contribute to circular economy objectives in the construction materials sector, with the potential to reduce both landfill burden and uncontrolled combustion emissions. Quantification of the waste utilization efficiency and lifecycle environmental performance through a dedicated LCA remains as future work. The reviewed literature [13] shows that some issues (fibre balling, loss of workability, high water demand, long-term swelling) can occur if a high dosage of DPF is present (DPF>1%). These issues are not within the scope of the current experiments.

5. Conclusion

The present study experimentally examined the physicochemical characterization of the combined use of sawdust ash (SDA) and alkali-treated date palm fiber (DPF) for the production of concrete with the intended goal of mechanical performance analysis and the establishment of regression equations. Compressive strength, split tensile strength, and flexural strength of three replicates were determined for each mix at 28, 56, and 90 days, following the relevant Indian Standards. The results presented here are all based on this campaign's experimental data only, and are the main conclusions:

- The three mechanical properties were shown to decrease systematically with the increase in SDA content above 10%. The compressive strength showed a reduction of 44.0% at 28 days, and the splitting strength and flexural strength showed a decrease of 41.7% and 49.0%, respectively, at 30% SDA. This is due to the predominance of cement dilution above a transition replacement level of around 10-15%.

- A 5% replacement SDA preserved (or slightly improved) strength at 28 days and increased compressive strength with a value of +4.0% in compressive strength, +7.5% in tensile strength, and +9.3% in flexural strength at 90 days compared to control, which is indicative of C–S–H formation. The materials used were therefore replaced with 5% SDA, which is identified as the optimum replacement.
- The gains in compression with alkali-treated DPF were relatively small (≤3.4%) when added to the optimum 5% SDA mix, while the gains in splitting tensile strength were relatively large (+19.5% to +45.9%), and the gains in flexural strength were very large (+62% to +111%). The optimum combined mix is 5% SDA + 1% DPF.
- Linear regression equations (Eqs. 4–12) yield R^2 values in the range of 0.85–0.96. Furthermore, the exponential models (Eqs. 13–21) exhibit R^2 values of 1.00. These equations may be used as interpolation tools within their applicable ranges and should not be extrapolated beyond the tested dosage limits. The proposed models provide a practical means of estimating the mechanical properties of SDA–DPF concrete mixtures within the investigated range of parameters and may serve as preliminary tools for mix design and performance prediction.
- The workability of all mix also reduced as the content of both SDA and DPF increased, but each mix was still workable without the use of a superplasticizer. The coefficient of variation was less than 5.2%, and the consistency was good in all cases.

5.1 Practical Implications

The 5% SDA + 1% DPF mixture will be able to valorize two abundant agricultural/industrial wastes, which will reduce the cement consumption by ~5% (including an embodied carbon reduction) and can be considered for applications requiring high flexural and tensile performance (overlays, secondary structural members, pavement slabs). These implications, however, are constrained to the mechanical performance data generated in this study. Deployment in structural applications requires completion of long-term durability testing, full LCA, cost–benefit analysis, and direct microstructural verification (SEM/EDS, MIP), all of which are identified as priorities for future work.

6. Limitations and future work

Only mechanical tests to evaluate mechanical strength for three curing ages are addressed in the present study. Full life-cycle and cost analyses, and direct microstructural verification (SEM/EDS, MIP, FTIR), have not been carried out and are a fundamental requirement prior to any deployment in structures. Future work will include (i) SEM/EDS and MIP testing to confirm the formation of C–S–H, refinement of the pores, and integrity of the fiber–matrix interface; (ii) complete LCA and cost–performance benchmark against conventional concrete; (iii) testing of durability indicators for a minimum of one year; (iv) scaling up the range of dosage for use of DPF (up to its onset of balling and to an upper, useful limit) and (v) investigating further alternative pozzolanic materials, such as metakaolin, silica fume, etc. to compensate for the reducing of the amount of cement and the use of a chemical activator. Conclusions therefore need to be taken with the reservation that they can only report the qualitative and order-of-magnitude estimates provided in Section 5.5 until further undertaken by the dedicated LCA study as provided as future work.

References

[1] Asif I, Hussain MU, Khan AA, Ashar M, Usman M, Shahid Z. Use of sawdust as an additive to cement in construction and study of its mechanical properties. Memorias de Investigaciones en Ingeniería. 2024; 26:54-69. https://doi.org/10.36561/ING.26.4

[2] Vantadori S, Zanichelli A, Carpinteri A, Luciano R. Structural integrity of shot-peened Ti-6Al-4V specimens under fretting fatigue. International Journal of Fracture. 2022;234(2):1-11. https://doi.org/10.1007/s10704-021-00523-0

[3] Ettu LO, Ezeh JC, Ibearugbulem OM, Anya UC, Njoku KO. Strength of binary blended cement composites containing cassava waste ash. International Journal of Emerging Technology and Advanced Engineering. 2013;3(4):15-20. https://doi.org/10.9790/3021-03444751

[4] Elinwa AU, Mahmood YA. Ash from timber waste as cement replacement. Cement and Concrete Composites. 2002;24(2):219-222. https://doi.org/10.1016/S0958-9465(01)00039-7
[5] Fahad F, Bhuiyan KI, Montasir F, Dey P, Akash MAA, Kumer A. Evaluating the use of eggshell powder and sawdust ash as cement replacements in sustainable concrete development. Journal of Sustainable Construction Materials and Technologies. 2025;10(1):1-21. https://doi.org/10.47481/jscmt.1667601
[6] Alatshan F, Altlomate AM, Mashiri F, Alamin W. Effect of date palm fibres on the mechanical properties of concrete. International Journal of Sustainable Building Technology and Urban Development. 2017;8(1):68-80.
[7] Adamu M, Alanazi F, Ibrahim YE, Alanazi H, Khed VC. A comprehensive review on sustainable natural fibre in cementitious composites: the date palm fibre case. Sustainability. 2022;14(11):6691. https://doi.org/10.3390/su14116691
[8] Said A, Ahmed S, Nabil M, Wontaser W. Production of hybrid fibre green concrete using date palm fibre and tyre wire waste. Case Studies in Construction Materials. 2024;20:e02851.
[9] AlSehali R, AlQaryan L, Alameri A, Althuwaimer R, Alnami R, Mustafaraj E. Untreated date palm fibres for sustainable reinforcement of cement mortars: a comparative study on structural and render applications. Journal of King Saud University - Engineering Sciences. 2025;37(6):28. https://doi.org/10.1007/s44444-025-00027-5
[10] Dehghan S, Hassani A. Experimental investigation of mechanical properties of roller-compacted concrete pavement (RCCP) reinforced with date palm fibres. Road Materials and Pavement Design. 2024;25(11):2549-2562. https://doi.org/10.1080/14680629.2024.2315072
[11] Ozerkan NG, Ahsan B, Mansour S, Iyengar S. Mechanical performance and durability of treated palm fibre reinforced mortars. International Journal of Sustainable Built Environment. 2013;2(2):131-142. https://doi.org/10.1016/j.ijsbe.2014.04.002
[12] Benaniba S, Driss Z, Djendel M, Raouache E, Boubaaya R. Thermo-mechanical characterisation of a bio-composite mortar reinforced with date palm fibre. Journal of Engineered Fibres and Fabrics. 2020; 15:1558925020948234. https://doi.org/10.1177/1558925020948234
[13] Zanichelli A, Carpinteri A, Fortese G, Ronchei C, Scorza D, Vantadori S. Contribution of date-palm fibres reinforcement to mortar fracture toughness. Procedia Structural Integrity. 2018;13:542-547. https://doi.org/10.1016/j.prostr.2018.12.089
[14] Kareche A, Agoudjil B, Haba B, Boudenne A. Study on the durability of new construction materials based on mortar reinforced with date palm fibre wastes. Waste and Biomass Valorisation. 2020;11(7):3801-3809. https://doi.org/10.1007/s10704-019-00669-y
[15] Hakkoum S, Kriker A, Mekhermeche A. Thermal characteristics of model houses manufactured by date palm fibre reinforced earth bricks in desert regions of Ouargla, Algeria. Energy Procedia. 2017;119:662-669. https://doi.org/10.1016/j.egypro.2017.07.093
[16] Wazzan AA. Effect of fibre orientation on the mechanical properties and fracture characteristics of date palm fibre reinforced composites. International Journal of Polymeric Materials. 2005;54(3):213-225. https://doi.org/10.1080/00914030390246379
[17] Ali-Boucetta T, Ayat A, Laifa W, Behim M. Treatment of date palm fibres mesh: influence on the rheological and mechanical properties of fibre-cement composites. Construction and Building Materials. 2021;273:121056. https://doi.org/10.1016/j.conbuildmat.2020.121056
[18] Dhull H. Effect on properties of concrete by using sawdust ash as partial replacement of cement. International Journal of Innovative Research in Science, Engineering and Technology. 2017;6(9):18603-18610.
[19] Elinwa AU, Ejeh SP, Mamuda AM. Assessing the fresh concrete properties of self-compacting concrete containing sawdust ash. Construction and Building Materials. 2008;22(6):1178-1182. https://doi.org/10.1016/j.conbuildmat.2007.02.004
[20] Majeed SS. Formulating eco-friendly foamed mortar by incorporating sawdust ash as a partial cement replacement. Sustainability. 2024;16(7):2612. https://doi.org/10.3390/su16072612
[21] Bureau of Indian Standards. IS 8112:1989. 43-Grade Ordinary Portland Cement - Specification. New Delhi: BIS; 1989.
[22] Bureau of Indian Standards. IS 1199:1959. Methods of sampling and analysis of concrete. New Delhi: BIS; 1959 (Reaffirmed 2018).
[23] Raheem AA, Olasunkanmi BS, Folorunso CS. Sawdust ash as partial replacement for cement in concrete. Organisation, Technology and Management in Construction: An International Journal. 2012;4(2):474-481. https://doi.org/10.5592/otmcj.2012.2.3
[24] Ibrahim YE, Adamu M, Marouf ML, Ahmed OS, Drmosh QA, Malik MA. Mechanical performance of date-palm-fibre-reinforced concrete containing silica fume. Buildings. 2022;12(10):1642. https://doi.org/10.3390/buildings12101642
[25] Marthong C. Sawdust ash (SDA) as partial replacement of cement. International Journal of Engineering Research and Applications. 2012;2(4):1980-1985.

[26] Benaimeche O, Carpinteri A, Mellas M, Ronchei C, Scorza D, Vantadori S. The influence of date palm mesh fibre reinforcement on flexural and fracture behaviour of a cement-based mortar. Composites Part B: Engineering. 2018;152:292-299. https://doi.org/10.1016/j.compositesb.2018.07.017
[27] Yousefi M, Khandestani R, Gharaei-Moghaddam N. Flexural behavior of reinforced concrete beams made of normal and polypropylene fibre-reinforced concrete containing date palm leaf ash. Structures. 2022; 37:1053-1068. https://doi.org/10.1016/j.istruc.2022.01.067
[28] Zhang P, Han S, Golewski GL, Wang X. Nanoparticle-reinforced building materials with applications in civil engineering. Advances in Mechanical Engineering. 2020;12(9):1687814020965438. https://doi.org/10.1177/1687814020965438
[29] Bentur A, Mindess S. Fibre Reinforced Cementitious Composites. 2nd ed. Boca Raton (FL): CRC Press; 2006. https://doi.org/10.1201/9781482267747
[30] Balea A, Fuente E, Monte MC, Blanco Á, Negro C. Fibre-reinforced cement-based composites. In: Fibre Reinforced Composites. Amsterdam: Elsevier; 2021. p. 597-648. https://doi.org/10.1016/B978-0-12-821090-1.00019-3
[31] Balaguru PN, Shah SP. Fiber-Reinforced Cement Composites. New York: McGraw-Hill; 1992.
[32] Banthia N. Fibre-reinforced concrete. In: ACI SP-142 Fibre Reinforced Concrete: Developments and Innovations. Farmington Hills (MI): American Concrete Institute; 1994. p. 91-119.
[33] Bamaga SO. A review on the utilisation of date palm fibres as inclusion in concrete and mortar. Fibres. 2022;10(4):35.
[34] Alawar A, Hamed AM, Al-Kaabi K. Characterisation of treated date palm tree fibre as composite reinforcement. Composites Part B: Engineering. 2009;40(7):601-606. https://doi.org/10.1016/j.compositesb.2009.04.018
[35] Bureau of Indian Standards. IS 516 (Part 1/Section 1):2018. Hardened concrete - Methods of test. New Delhi: BIS; 2018.
[36] Mageswari M, Vidivelli B. The use of sawdust ash as fine aggregate replacement in concrete. Indian Journal of Environmental Research and Development. 2009;3(3):720-726.
[37] Bureau of Indian Standards. IS 3812 (Part 1):2003. Pulverised fuel ash - Specification. New Delhi: BIS; 2003.
[38] Bureau of Indian Standards. IS 10262:2019. Concrete mix proportioning - Guidelines. New Delhi: BIS; 2019.
[39] Bureau of Indian Standards. IS 5816:1999. Splitting tensile strength of concrete - Method of test. New Delhi: BIS; 1999.

Appendix: List of Abbreviations

S.No.	Abbreviation	Description
1	SDA	Sawdust ash
2	DPF	Date palm fibre
3	OPC	Ordinary Portland cement
4	PC / H0	Plain (control) concrete with 0% SDA
5	H5%	Concrete with 5% SDA replacement
6	H10%	Concrete with 10% SDA replacement
7	H20%	Concrete with 20% SDA replacement
8	H30%	Concrete with 30% SDA replacement
9	DPF 0.5%	Concrete with 5% SDA + 0.5% treated DPF
10	DPF 1%	Concrete with 5% SDA + 1.0% treated DPF
11	C–S–H	Calcium silicate hydrate
12	$Ca(OH)_2$	Calcium hydroxide (portlandite)
13	w/b	Water-to-binder ratio
14	SD	Standard deviation
15	CV	Coefficient of variation
16	R^2	Coefficient of determination
17	SSD	Saturated surface-dry condition
18	LCA	Life-cycle assessment
19	SEM/EDS	Scanning electron microscopy / Energy-dispersive spectroscopy
20	MIP	Mercury intrusion porosimeter